Uncompensated Moments in the MnPd/Fe Exchange Bias System

Sebastian Brück,* Gisela Schütz, and Eberhard Goering
Max-Planck-Institut für Metallforschung, Heisenbergstrasse 3, D-70569 Stuttgart, Germany

Xiaosong Ji and Kannan M. Krishnan+
Department of Materials Science and Engineering, University of Washington, Seattle, Washington 98195, USA
(Received 8 July 2008; published 16 September 2008)

The element-specific magnetic structure of an epitaxially grown $Mn_{52}Pd_{48}$/Fe bilayer showing exchange bias was investigated with atomic-layer depth sensitivity at the antiferromagnet/ferromagnet interface by soft-x-ray magnetic circular dichroism and magnetic reflectivity. A complex magnetic interfacial configuration, consisting of a 2-monolayer-thick induced ferromagnetic region, and pinned uncompensated Mn moments that reach far deeper (~13 Å), both in the antiferromagnet, were found. For the latter, a direct relationship with the magnitude of the exchange bias is verified by similar measurements perpendicular to the field cooling direction.

DOI: 10.1103/PhysRevLett.101.126402 PACS numbers: 71.70.Gm, 75.70.Cn, 61.05.cm

A material system composed of a ferromagnet (FM) in direct contact with an antiferromagnet (AFM) shows a shift of the hysteresis loop when cooled in an external field through the Néel temperature of the AFM. This effect is called exchange bias (EB) since the observed shift can be described by an intrinsic biasing field induced by the AFM via coupling across the interface [1,2]. In a very intuitive picture, uncompensated AFM spins at the interface couple to the FM thus inducing an additional resistance to the reversal of the FM. In this picture, if the uncompensated AFM spins involved are free, it generally results in an enhancement in coercivity; on the other hand, if the AFM spins involved are pinned, it results in an additional unidirectional anisotropy or EB. However, the experimentally observed effect differs by orders of magnitude from the predictions of this simple model. To overcome the discrepancy, several alternative models of EB, mostly based on a weakening of the AFM by domain formation, have been developed [3–7]. Recent experimental results [8] point more and more towards the interface and its magnetic configuration as the main parameter for EB. Element-selective x-ray techniques [9,10], for example, revealed the existence of induced ferromagnetism in the AFM layer in various EB systems [11–14]. Such induced ferromagnetism complicates simple theoretical descriptions since most models so far introduce a clear structural demarcation between the FM and AFM layers. The presence of ferromagnetism in the AFM immediately raises the question of where the pinned moments which are responsible for the anisotropy are located. It is obvious that further understanding can be achieved only by obtaining a precise atomic scale mapping of the interfacial magnetic configuration for each element involved. The fact that the interface is deeply buried in the sample limits the available techniques to neutron and x-ray scattering or spectroscopy. Especially, soft-x-ray resonant magnetic reflectometry (XRMR) has been demonstrated to be a powerful method for investigating magnetism at buried interfaces [14,15]. From the angular-dependent reflectivity for x rays, it is possible to derive information on the chemical or structural properties of the sample. This method can be extended by using circular polarized light and measuring at a magnetic active absorption edge such as the L edges of the transition metals. In this case, the scattering process becomes dependent on the scalar product $\vec{P} \cdot \vec{M}$ of the circular polarization $\vec{P}$ and the magnetization $\vec{M}$ in the sample, thus introducing a magnetic asymmetry to the reflectivity spectra [16]. From the analysis of the circular dichroic reflectivity spectra, it is possible to obtain the magnetic as well as the chemical or structural profile of the sample with very high precision [15]. Here this technique has been used to determine with atomic layer depth sensitivity the magnetic configuration at the interface of an epitaxially grown, metallic, FM/AFM system and correlate it with its EB behavior.

A bilayer sample with nominal thicknesses of $Mn_{52}Pd_{48}$(750 Å)/Fe(85 Å)/Pt(15 Å) was grown epitaxially on a MgO(001) substrate in an ultrahigh vacuum ion-beam sputter deposition system with a base pressure of 10^{-9} mbar. $Mn_{52}Pd_{48}$ is an antiferromagnet with a Néel temperature of $T_N \approx 500$ K for this composition and a CuAu-I-type crystal structure [17]. By controlling the substrate temperature during growth, it is possible to control the structural properties of the MnPd including its crystallographic orientation relationship with respect to the substrate [18,19]. Specifically, the sample investigated was grown at a substrate temperature of 85°C, which leads to chemically disordered MnPd. By a subsequent annealing at 250°C for 1 h in vacuum, a chemically ordered phase is formed which exhibits a very good crystallographic orientation relationship such that its a axis is normal to the film. Besides, a magnetic field is applied during the annealing process to induce a well-defined uniaxial anisotropy along the Fe[100] direction. The crystallographic a-axis orientation of the sample was verified by x-ray diffraction [18,19].

The XMCD (x-ray magnetic circular dichroism) and XRMR investigations were carried out at the UE56/2-PGM1 beam line at BESSY II in Berlin, Germany, using a dedicated 3-axis diffractometer setup optimized for magnetic reflectivity investigations [20]. The postprocessing of the reflectivity data was performed using software capable of simulating arbitrary magnetic reflectivities. The algorithm is based on the so-called magneto-optical approach [21] in combination with multislicing to account for roughness [15].

Magnetic properties, especially the magnitude of EB, were characterized during the XRMR investigation by measuring element-selective hysteresis in reflection. The sample was set to an angle of incidence Θ with pronounced magnetic asymmetry, and the specular reflected beam was measured as a function of the applied field. The normalized hysteresis loop as obtained from measuring at the Fe L_3 edge is shown in Fig. 1. A room temperature EB of $H_E = -4.5$ mT and a coercive field of $H_C = 12.1$ mT, consistent with room temperature vibrating sample magnetometry measurements of the same sample, were found.

The optical constants were obtained by measuring x-ray absorption spectra of the relevant Fe- and Mn-L edges. From the measured absorption, i.e., the absorptive part β, the corresponding dispersive part δ of the optical constants was calculated using the Kramers-Kronig relation. In order to probe the chemical depth profile, i.e., roughness and thickness of the layers, nonmagnetic resonant reflectivity curves were measured using linear polarized x rays. The reflectivity curve measured at the maximum of the L_3 edge of Mn at 639.5 eV is shown as an inset in the upper left of Fig. 2. A strong nearly undamped oscillation is found which corresponds to interference between reflections from the sample surface and from the Fe/MnPd interface. To properly determine roughness and absorption in the sample, a simulated curve based on the above-mentioned magneto-optical approach is fitted to the measurement. The simulated reflectivity, shown in the inset as a solid red line, is in perfect agreement with the measured curve. From the resonant nonmagnetic reflectivity, the following thickness and roughness parameters are found: Pt(16.4 Å)/Fe(87.3 Å)/$Mn_{52}Pd_{48}$(750 Å); the relevant

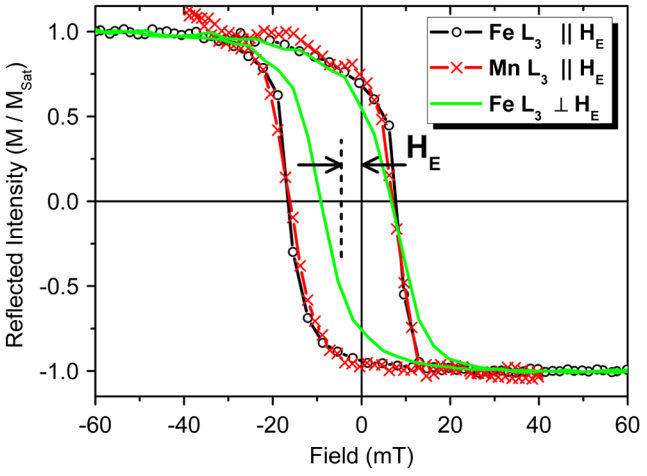

FIG. 1 (color online). Hysteresis loops for Fe and Mn measured in reflection parallel and perpendicular to the Fe[100] or exchange bias direction. The Fe hystereses along (○) and perpendicular to H_E (solid line) are measured at an energy of 707.2 eV and at an angle of incidence of $\Theta = 11°$. The Mn hysteresis (×) parallel to H_E is measured at 639.5 eV and $\Theta = 9.5°$. Mn and Fe exhibit a strong coupling which can be seen from the similar shape of the respective hystereses.

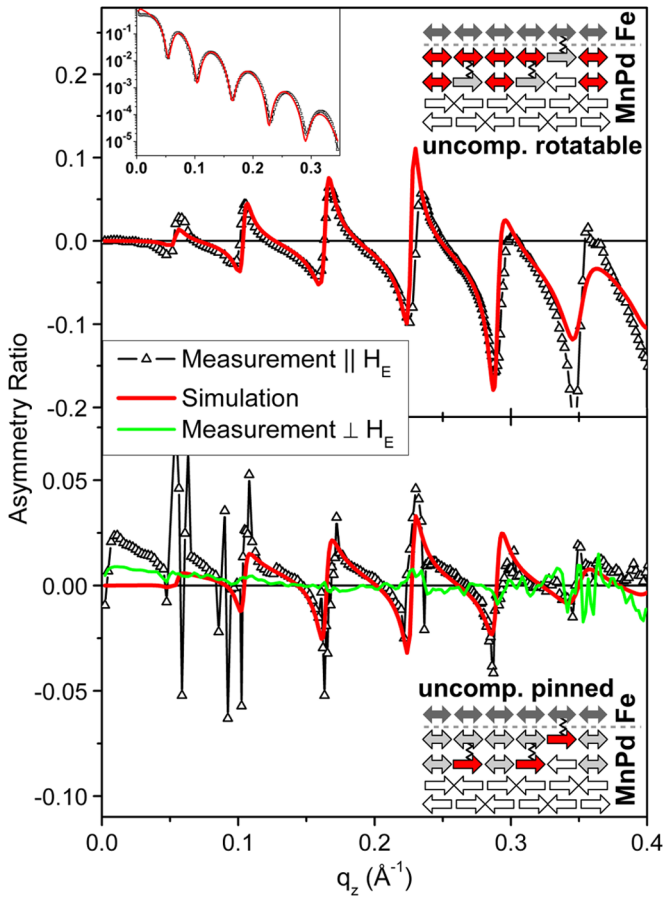

FIG. 2 (color online). Magnetic asymmetries for both types of Mn moments in the sample. The upper graph is the conventional ferromagnetism-caused asymmetry as obtained from flipping the magnetization in the sample. The presence of the Fe induces ferromagnetism in the very first layers of the AFM which is oriented antiparallel with respect to the magnetization of the Fe at the interface. The inset on the upper left shows the reflectivity curve as obtained by measuring with horizontal linear polarized light along with the corresponding fit result. From this curve, structural, i.e., chemical, properties have been deduced. The lower graph shows the *pinned asymmetry* which corresponds to pinned uncompensated moments in the AFM. A possible scenario for interfacial Mn moments and their respective coupling mechanisms is illustrated by the two sketches. Rotatable moments (Mn or Fe) are represented by double arrows. The springs illustrate possible couplings between the pinned Mn and the rotatable Mn and Fe. Highlighted in red are the moments probed by the respective asymmetry.

MnPd/Fe interface roughness is $\sigma_{\mathrm{RMS}} = 1.8$ Å. The corresponding optical profile at the MnPd/Fe interface is shown in Fig. 3. It is noteworthy that analogous measurements of the reflectivity at the Fe L_3 edge and Mn L_2 edge yield similar values.

Circular dichroic, i.e., magnetic, reflectivity spectra were measured at the Mn L_3 edge to probe the existence of rotatable and pinned uncompensated Mn moments in the AFM. By measuring the reflected intensity at every angle for parallel and antiparallel magnetic fields, high-quality XRMR spectra have been obtained for both circular polarizations of the incident x rays. From the curves, the magnetic asymmetry related to rotatable Mn moments has been calculated according to $A = (I_N^+ - I_S^+)/(I_N^+ + I_S^+)$, where N and S refer to the direction of the magnetic field with respect to the incident beam direction. N corresponds to parallel alignment with positive circular light and S to antiparallel alignment. The upper part of Fig. 2 shows the resulting Mn magnetic asymmetry ($\triangle$) as measured at an energy of 639.5 eV (maximum L_3).

A pronounced asymmetry of up to 20% is found, clearly proving the existence of rotatable Mn moments in the sample. To answer the question of where these rotatable Mn moments are located, i.e., at the interface or in the bulk, the asymmetry curve has been fitted using the above-mentioned magneto-optical simulation technique. Making use of the already known structural information, the circular dichroic contribution was simulated using a Gaussian-shaped distribution of localized magnetic moments. The moment was set to $\sim 1.2\mu_B$ per Mn atom corresponding to values found in ultrathin Mn layers on top of a ferromagnetic substrate [22,23]. The final fit is plotted in the upper graph of Fig. 2 as a solid line (red online). As can be seen, the measured asymmetry is reproduced perfectly by the simulation. The magneto-optical profile of the rotatable Mn moments is shown in Fig. 3 as dashed lines ($\delta_{\mathrm{rotatable}}$ and $\beta_{\mathrm{rotatable}}$ as green and blue, respectively). Please note that the corresponding magneto-optical constants $\delta_{\mathrm{rotatable}}$ and $\beta_{\mathrm{rotatable}}$ have been multiplied by a factor of 20 for better visibility. Rotatable Mn moments are found only in a narrow region of 4 Å width directly at the interface to Fe. This corresponds to roughly two monolayers of MnPd and correlates with the roughness of the MnPd/Fe interface which is 3.6 Å (FWHM). The general decrease of the Mn density at the interface due to the chemical profile results in a cutoff and, respectively, a steeper slope at the right side of the rotatable moment distribution. The maximum of the rotatable moments lies ~ 1 Å below the nominal interface position. By comparing the resulting absorptive part of the rotatable Mn with the corresponding XMCD of Fe (not shown here), antiferromagnetic coupling between Fe and Mn is found.

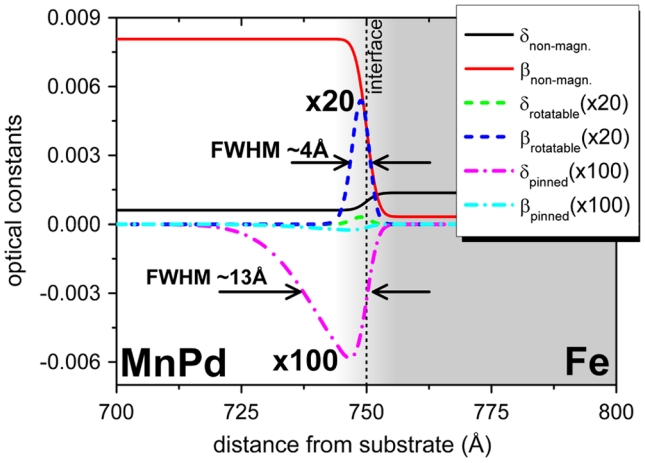

FIG. 3 (color online). Optical and magneto-optical profile of the sample showing the situation directly at the AFM/FM interface. All profiles have been measured at the same energy of 639.5 eV. The optical profiles corresponding to the structural information from the nondichroic reflectivity are shown as red and black solid curves. Rotatable Mn moments lead to the $\delta_{\mathrm{rotatable}}$ (dashed green curve) and $\beta_{\mathrm{rotatable}}$ (dashed blue curve) profile. The values have been multiplied by 20 for better visibility. The pinned Mn moments lead to the magneto-optical profile given by δ_{pinned} (dashed-dotted magenta curve) and β_{pinned} (dashed-dotted light-blue curve). Both values have been multiplied by 100.

To further explore the nature of these rotatable moments, their magnetization reversal was investigated using element-selective magnetic reflectivity. Therefore the specular reflection at the Mn L_3 edge at an angle of incidence of $\Theta = 9.5°$ (corresponding to $q_z = 0.107$ Å^{-1}) has been measured while varying the external field from positive to negative saturation. The result, shown in Fig. 1, is a typical ferromagnetic hysteresis loop which follows the corresponding Fe hysteresis. The fact that the induced ferromagnetism is strongly located at the interface along with the similar shape of the Mn and Fe hysteresis loops is a clear indication that the short range interaction from the Fe dominates the Mn behavior. In the upper right of Fig. 2, a sketch illustrates the possible magnetic configuration at the interface. Because of the Fe and the accompanying presence of a strong magnetic coupling, neighboring Mn atoms are forced to rotate with the ferromagnet instead of coupling to the AFM spin lattice. However, the relative orientation of the Fe and Mn rotatable moments is antiparallel. This interpretation is supported by neutron reflectivity investigations of MnPd which showed that the antiferromagnetic spin lattice is very sensitive to changes in stochiometry and/or ferromagnetic additions [17].

The unidirectional anisotropy, i.e., the EB in the sample, has to be related to pinned uncompensated moments in the AFM. Such pinned moments are not visible from the usual asymmetry as it is described above since it is sensitive only to rotatable contributions. Instead, a new asymmetry, referred to as pinned asymmetry, according to the following scheme will be used: $\hat{A} = (I_N^+ - I_S^-)/(I_N^+ + I_S^-)$. Note how the field is always parallel to the helicity $\vec{P}$ since the helicity changes sign. This pinned asymmetry probes magnetic uncompensated contributions which do not rotate

while blanking out all rotatable parts. The pinned asymmetry for the Mn L_3 edge, as it has been obtained by applying the above described calculus, is shown in the lower graph of Fig. 2 as open triangles. A small signal of 2.5% is found which is roughly 10 times smaller than the rotatable contribution. To identify the location of the pinned Mn moments in the AFM, the same simulation and refinement process described for the normal asymmetry has been used. The final result of the fitting process is shown in the lower graph of Fig. 2 together with the measurement. Although the signal is nearly 5 times smaller than the one from the rotatable Mn, good agreement of simulation and measurement is found. The contribution of the pinned uncompensated Mn moments to the magneto-optical constants is plotted in Fig. 3 as dashed-dotted lines (δ_{pinned} as magenta and β_{pinned} as light-blue line, respectively). As expected from the different magnitudes, the contribution is several times smaller than the one from the rotatable part. It is found that pinned Mn moments occur in a much wider region of 13 Å (FWHM) in width with the maximum of the pinned moment distribution ~2 Å below the maximum for the rotatable moments. Here the cutoff effect caused by the interface (chemical profile) is even more pronounced. Moreover, the magneto-optical constants of the pinned moments show an unexpected behavior: While one would expect a large absorptive part β_{pinned}, since the measurement is carried out at the maximum of the L_3 edge, the simulation yields, on the contrary, a very large dispersive part δ_{pinned} and only a small absorption. This effect might result from a modified shape and/or position of the magnetic spectra of the pinned Mn atoms as it is imposed, for example, by a change of the local chemical environment. The coupling of the pinned moments is estimated by comparing the sign of the magneto-optical constants with ferromagnetic metallic Mn reference data; see, for example, [22]. More details on this evaluation will be described elsewhere [24]. The coupling is found to be parallel to the Fe but antiparallel to the rotatable Mn which is compatible with the expected spin configuration of a-axis MnPd [18]. In contrast, antiparallel coupling has been reported in CoO and IrMn [25]. This might result from the different spin structure of these antiferromagnets compared to the one in MnPd.

EB is a unidirectional effect which goes through a minimum when measuring perpendicular to the bias direction. Accordingly, the projections of the associated pinned moments along the beam direction should show a similar angular dependency. To verify the direct relationship of the pinned Mn moments identified here to the EB, the sample has been rotated azimuthally by 90°. Then an element-selective hysteresis in reflection, similar to the one described above, has been measured at the Fe L_3 edge (E = 707.2 eV, $\Theta = 11°$), and the result is shown in Fig. 1 as a solid (green) curve. A small remaining bias of $H_E = -1.2$ mT and a coercive field of $H_C = 8$ mT is found perpendicular to the direction of EB. Next, the magnetic reflectivity was measured for the same energy of 639.5 eV at the Mn L_3-edge maximum similar to the parallel measurement. The corresponding pinned asymmetry is plotted in the lower graph of Fig. 2 as a solid green line. As expected, the pinned asymmetry, i.e., the signal from pinned uncompensated moments, is strongly reduced, providing direct evidence for the relation of pinned asymmetry and exchange bias.

From these findings, we can now derive a precise picture of the magnetic configuration at the interface: The Mn atoms which have Fe as neighbors couple to them but align antiparallel to the Fe moments. This coupling is so strong that the Mn follows perfectly the Fe hystereses and exhibits identical anisotropy or coercivity. In other words, it can be seen as an antiparallel extension of the FM by one monolayer. Pinned Mn moments are found mostly below the rotatable ones, and they couple ferromagnetically to the Fe. In other words, they are aligned antiferromagnetically to the rotatable Mn. The situation is illustrated by the two sketches in Fig. 2 for rotatable and pinned uncompensated Mn moments, respectively.

The authors thank V. Ferreras Paz, B. Zada, and W. Mahler for support during the beam time at BESSY II. Work at UW was supported by DoE/BES under Contract No. ER45987

*brueck@mf.mpg.de
+kannanmk@u.washington.edu

[1] W. H. Meiklejohn *et al.*, Phys. Rev. **105**, 904 (1957).
[2] A. E. Berkowitz *et al.*, J. Magn. Magn. Mater. **200**, 552 (1999).
[3] M. Kiwi, J. Magn. Magn. Mater. **234**, 584 (2001).
[4] U. Nowak *et al.*, Phys. Rev. B **66**, 014430 (2002).
[5] A. P. Malozemoff, Phys. Rev. B **35**, 3679 (1987).
[6] N. C. Koon, Phys. Rev. Lett. **78**, 4865 (1997).
[7] T. C. Schulthess *et al.*, Phys. Rev. Lett. **81**, 4516 (1998).
[8] W. Kuch *et al.*, Nature Mater. **5**, 128 (2006).
[9] G. Schütz *et al.*, *Handbook of Magnetism and Advanced Magnetic Materials* (Wiley, New York, 2007), Vol. 3.
[10] G. Srajer *et al.*, J. Magn. Magn. Mater. **307**, 1 (2006).
[11] F. Offi *et al.*, Phys. Rev. B **67**, 094419 (2003).
[12] H. Ohldag *et al.*, Phys. Rev. Lett. **96**, 027203 (2006).
[13] S. Brück *et al.*, J. Magn. Magn. Mater. **310**, 2316 (2007).
[14] M. R. Fitzsimmons *et al.*, Phys. Rev. B **75**, 214412 (2007).
[15] J. Geissler *et al.*, Phys. Rev. B **65**, 020405(R) (2001).
[16] J. P. Hannon *et al.*, Phys. Rev. Lett. **61**, 1245 (1988).
[17] L. Pál *et al.*, J. Appl. Phys. **39**, 538 (1968).
[18] N. Cheng *et al.*, J. Appl. Phys. **89**, 6597 (2001).
[19] P. Blomqvist *et al.*, J. Appl. Phys. **95**, 8019 (2004).
[20] S. Brück *et al.*, Rev. Sci. Instrum. **79**, 083109 (2008).
[21] J. Zak *et al.*, Phys. Rev. B **43**, 6423 (1991).
[22] W. L. O'Brien *et al.*, Phys. Rev. B **50**, 2963 (1994).
[23] E. Goering *et al.*, Appl. Phys. A **78**, 855 (2004).
[24] S. Brück *et al.* (unpublished).
[25] I. Schmid *et al.*, Europhys. Lett. **81**, 17 001 (2008).